Scientific Research Publishing

Open Journal of Marine Science, 2025, 15(3), 129-156
https://www.scirp.org/journal/ojms
ISSN Online: 2161-7392
ISSN Print: 2161-7384

Modeling Seabed-Origin Oil Spills Using OpenOil: Case Studies from the Mediterranean Sea

Vassilios Papaioannou, Christos G.E. Anagnostopoulos, Konstantinos Vlachos, Anastasia Moumtzidou, Ilias Gialampoukidis, Stefanos Vrochidis, Ioannis Kompatsiaris

Information Technologies Institute, Centre for Research and Technology Hellas, Thessaloniki, Greece
Email: vaspapa@iti.gr, anagn_c@iti.gr, kostasvlachosgrs@iti.gr, moumtzid@iti.gr, heliasgj@iti.gr, stefanos@iti.gr, ikom@iti.gr

How to cite this paper: Papaioannou, V., Anagnostopoulos, C.G.E., Vlachos, K., Moumtzidou, A., Gialampoukidis, I., Vrochidis, S. and Kompatsiaris, I. (2025) Modeling Seabed-Origin Oil Spills Using OpenOil: Case Studies from the Mediterranean Sea. *Open Journal of Marine Science*, **15**, 129-156.
https://doi.org/10.4236/ojms.2025.153008

Received: May 20, 2025
Accepted: July 7, 2025
Published: July 10, 2025

Abstract

Seabed-origin oil spills pose distinct challenges in marine pollution management due to their complex transport dynamics and weathering processes. This study applies the OpenDrift's OpenOil module to simulate the transport and fate of oil in two seabed-origin spill scenarios: (a) the 2019 Baniyas refinery spill in Syria, resulting from leakage in underwater pipelines, and (b) a natural oil seep near Zakynthos, Greece (2017), where hydrocarbons naturally escape from the seafloor. The Baniyas spill was used as a validation case, integrating Sentinel-2 satellite imagery and open-source atmospheric and marine data derived from the Climate Change and Copernicus Marine services to refine model calibration. The Zakynthos seep was analyzed under controlled conditions to assess the abilities of the OpenOil module to simulate naturally occurring oil slicks. Key findings indicate that oil density plays a critical role in evaporation dynamics. Simulations revealed that oils above a specific density threshold showed negligible evaporation, remaining as persistent slicks in the water column, whereas lighter oils exhibited substantial evaporation rates, significantly altering their dispersion behavior.

Keywords

Seabed Oil Spill, Oil Weathering, Openoil, Numerical Simulations, Lagrangian Modeling, Mediterranean Spills

1. Introduction

Oil spills occur from natural leaks, oil transportation, drilling, and accidents involving tankers, pipelines, and rigs. While smaller spills are easier to manage, large

spills pose significant challenges. According to the International Tanker Owners Pollution Federation (ITOPF) [1], oil spills in the Mediterranean Sea have totaled approximately 540,000 tons. Public attention often focuses on major spills, overlooking frequent smaller ones [2]. Data from the ITOPF [1], shows that over 80% of recorded spills since 1970 were small (under 7 tons). Additionally, 250,000 tons of oil are lost annually from ship operations, with another 120,000 tons spilled near refineries and terminals. Incomplete data on accidental spills highlights the urgent need for better detection and monitoring systems.

Oil pollution does not remain on the sea surface—it can spread to deeper waters, worsening its environmental impact. The extraction of oil from deep-water reservoirs and the installation of pipelines at great depths increase the risk of spills from well blowouts or pipeline leaks [3]. Notable deep-water spills include the 2010 Deepwater Horizon disaster in the Gulf of Mexico, which released an estimated 492,000 to 627,000 tons of oil [4], and the 2011 Penglai 19-3 spill in the Bohai Sea, China, which spilled about 200 tons [5].

The behavior of an oil spill in the ocean is influenced by physical, chemical, and biological processes. These depend on factors such as oil type, environmental conditions (waves, wind, currents, sunlight), and release method (sudden or continuous, surface or deep water). Oil weathering processes—spreading, evaporation, emulsification, dissolution, photo-oxidation, biodegradation, and sedimentation—strongly affect the spill's fate. Additionally, physical processes like transport, turbulent mixing, dispersion, and resurfacing play key roles in its movement and spread [6] [7].

When oil spills into the sea, it undergoes changes as it interacts with the environment. The first process, spreading, occurs as the oil forms a thin film that expands across the surface. Factors like sea surface temperature, oil viscosity, and density influence how quickly and thick the slick becomes [8] [9]. Models estimate these properties, which are crucial for predicting subsequent processes like evaporation, dispersion, and emulsification. Evaporation quickly follows, as lighter components of the oil diffuse into the air. Within hours, these volatile fractions evaporate, leaving behind heavier, more persistent oil, which also reduces toxicity in the water [10]. Emulsification can occur as waves mix water into the oil, creating a sticky "mousse." This depends on the oil's viscosity, composition, and temperature. Higher viscosity oils are more likely to form emulsions, slowing evaporation and complicating cleanup [11]. Over time, biodegradation begins, as microorganisms break down the oil into less harmful substances. Though once seen as slow, research after the Deepwater Horizon spill showed that biodegradation can start within a week, aiding natural cleanup [12] [13].

OpenDrift is an open-source Python framework developed by the Norwegian Meteorological Institute for Lagrangian particle modeling. Its flexible design supports various applications, such as oil drift, search and rescue, pelagic egg tracking, and atmospheric drift [14]. One key application was by [15], who used high-resolution models to study how riverfronts affected oil slick transport during the

2010 Deepwater Horizon spill. Using satellite data and the Gulf of Mexico Hybrid Coordinate Ocean Model (GoM-HYCOM) along with European Centre for Medium-Range Weather Forecasts (ECMWF) products, their simulations showed that river-induced fronts significantly impacted the amount and location of stranded oil. In another study, [16] used OpenDrift and high-resolution ocean data to examine oil transport and fate over six years, focusing on the influence of circulation patterns like the Loop Current and mesoscale dynamics in the Straits of Florida. While OpenOil offers modularity and Lagrangian flexibility, it is worth comparing its capabilities with other operational models like MEDSLIK II. MEDSLIK II, widely used in the Mediterranean, focuses on both surface and subsurface spills and incorporates advection, diffusion, and oil weathering processes [17]. Compared to MEDSLIK II, OpenOil offers finer vertical resolution and more customizable droplet physics through lognormal distributions. Additionally, OpenOil can better simulate vertical dynamics critical for seabed-origin spills, a key requirement in this study [17].

For this purpose, this study explores the application of OpenDrift's OpenOil module to simulate the transport and fate of oil in two distinct spill scenarios: the 2019 Baniyas refinery oil spill in Syria and a natural oil seep near Zakynthos, Greece. The primary objective is to assess the capability of OpenOil for simulating oil spill behavior in complex marine environments, with a focus on seabed-origin oil spills. The study builds upon calibration and validation using the Baniyas refinery spill and extends the analysis to Zakynthos to investigate the behavior of naturally occurring oil slicks and test model performance under varying environmental and oil type conditions.

The Baniyas refinery spill occurred in June 2019 due to leakage of underwater oil pipelines near the Baniyas oil terminal. This led to a large crude oil release, with the spill spreading over 22 kilometers along Syria's northern coast and affecting areas up to 100 kilometers away, including Latakia [18]. The Baniyas refinery processes 6 million metric tons of crude oil annually and is vital for Syria's oil-dependent economy. The spill's seabed-origin nature, combined with infrastructure damage, underscores the region's vulnerability to marine pollution. Narrow coastal zones, weak eastern Mediterranean currents, and fluctuating winds further complicate oil dispersion. Past oil-related incidents have caused severe environmental damage, highlighting the need for accurate spill modeling and effective response strategies [17].

Zakynthos Island, located in the Ionian Sea, is known for natural oil seeps, especially along its southern coast. These seeps create recurring oil slicks up to 15 kilometers long, driven by geological processes [19]. The calm sea conditions during summer, with low winds and moderate currents, provide ideal conditions for studying oil slick dynamics and testing model performance. Zakynthos also hosts high biodiversity and marine protected areas, emphasizing the need to monitor and reduce the potential impact of oil pollution on sensitive ecosystems [20]. The predictable nature of the Zakynthos seep makes it a valuable case study for vali-

dating oil spill models and comparing natural and anthropogenic spill behaviors.

The selection of these two study areas is driven by their unique seabed-origin spill characteristics, which pose distinct challenges compared to surface-origin spills. Seabed-origin spills involve oil transport through the water column, delayed detection, and complex interactions with oceanographic and weathering processes. By investigating these scenarios, this study aims to fill a gap in oil spill modeling research and enhance understanding of oil behavior in these environments. The Baniyas spill represents the risks associated with aging infrastructure and geopolitical instability, while the Zakynthos seep offers insight into the natural dynamics of oil spills, providing a contrasting case to anthropogenic events. Together, these cases allow for a comprehensive evaluation of OpenOil's performance and its ability to predict oil transport and fate under varying conditions.

Overall, special emphasis is given to the following questions:

- How accurately can OpenOil model the transport and fate of oil in a seabed-origin spill, such as the Baniyas refinery spill?
- To what extent can parameters calibrated from the Baniyas spill be applied to other scenarios, such as the Zakynthos natural oil seep?
- How do oil type and density affect spill behavior, particularly evaporation, spreading, and persistence in the marine environment?

2. Methodology

The methodology section outlines the approach used to model and analyze oil transport and dispersion. It begins with an overview of the OpenOil model and its requirements, followed by a discussion of the physical properties and governing equations that describe horizontal and vertical transport processes. Finally, the numerical simulation setup is detailed, including study areas such as Baniyas, Syria, for validation and Zakynthos, Greece for further analysis.

2.1. OpenOil Model and Its Requirements

For this study, we use OpenDrift's OpenOil module to simulate how oil spreads and changes over time in two different spill events: the 2019 Baniyas refinery oil spill in Syria and a natural oil seep near Zakynthos, Greece. The simulation employs the OpenOil model, which combines oil spill transport and weathering simulation with real-time meteorological and oceanographic forecasts. OpenOil, a component of the broader open-source particle trajectory framework called OpenDrift [14], represents released oil as individual particles with specific characteristics like mass, viscosity, and density, collectively known as Lagrangian elements.

Each oil particle's movement is influenced by factors such as current, wind, and Stokes drift, while random walk schemes are also incorporated to model diffusion due to turbulence. The model integrates various physical processes including wave entrainment [21], turbulence-induced vertical mixing [22], oil resurfacing due to buoyancy [23], and emulsification [24]. Oil resurfacing is parameterized based on

oil density and droplet size, with sinking velocity determined by Stokes Law, making the model sensitive to the initial oil droplet size distribution [15].

Oil properties utilized in OpenOil are sourced from the Automated Data Inquiry for Oil Spills (ADIOS) database, which contains measured properties of nearly 1000 oil types worldwide [25]. To enhance accuracy, the OpenOil model is forced with wind data, ocean currents and waves. One key dataset is the ERA5 reanalysis dataset, produced by ECMWF. ERA5 provides hourly weather data, including wind speed and direction at 10 meters above the surface [26]. Specifically, it includes two key variables: u_{10m}, which represents wind moving eastward, and v_{10m}, which represents wind moving northward. These values come from a combination of past observations and computer model simulations.

Another important dataset is the Med MFC Physical Multiyear Product, which offers detailed information on the physical state of the Mediterranean Sea. This dataset is created using the Nucleus for European Modelling of the Ocean (NEMO) hydrodynamic model along with a data assimilation method called OceanVAR. It combines various ocean measurements, such as ocean current, temperature and salinity, with satellite data on sea level changes. The dataset has a high-resolution grid, covering the Mediterranean Sea with a spacing of about 4 - 5 km. It also includes 141 layers of ocean depth, providing a detailed view of underwater conditions [27].

Finally, for wave conditions, the study uses the Med-WAV Mediterranean Sea Waves Product [28]. This dataset consists of key wave variables such as significant wave height, mean and peak wave period, wave direction, wind sea and swell components, and the wave energy spectrum. It provides a high spatial resolution of 1/24˚ (approximately 5 km), covering the Mediterranean Sea and extending into the Atlantic Ocean up to 18.125˚ W. To enhance accuracy, the dataset incorporates an optimal interpolation data assimilation method, which integrates satellite observations of wave height with wind data from ERA5, ensuring reliable wave forecasts and historical analyses.

2.2.1. Horizontal Transport

Oil elements are subject to advection by currents, wind, and waves, which collectively influence their horizontal motion. Whether submerged or at the surface, oil particles follow the ambient current, experience wind drift—crucial for their horizontal movement—which typically ranges from approximately 1% to 6% of the surface wind speed, often around 3%. Additionally, they are affected by the surface Stokes drift, with its profile calculated by [29] based on the Phillips spectrum.

2.2.2. Vertical Transport

A) Wave entrainment: Wave entrainment refers to how particles in the water move during stormy conditions and when waves break in the open sea. The mixing of oil near the surface in open seas largely depends on the energy from the breaking waves [30]. To better understand wave entrainment, several factors are considered, such as the thickness, density, and viscosity of the oil, the oil-water

surface tension, water density, gravity, the energy available from breaking waves to lift the oil, and the extent of the sea surface affected by breaking waves [31]. A formula for the rate of oil entrainment, Q, is given by two dimensionless numbers: Weber (We) and Ohnesorge (Oh). The formula is (Equation 1):

$$Q = Q_0 F_{bw} \tag{1}$$

- where: F_{bw} is the fraction of the sea surface with breaking waves, and Q_0 is the dimensionless vertical oil flux from the sea surface into the water column, calculated by Equation 2:

$$Q_0 = aWe^b Oh^c \tag{2}$$

- where: $a = 4.604 \times 10^{-10}$, $b = 1.805$, and $c = -1.023$ according to [32]. So, the Equation 1. becomes:

$$Q = 4.604 \times 10^{-10} We^{1.805} Oh^{-1.023} F_{bw} \tag{3}$$

- where: F_{bw} is related to the wind speed and wave period (the time between waves) based on [33], and is calculated as:

$$F_{bw} = \begin{cases} a_{bw} \dfrac{U_{10m} - U_o}{T_p}, if\ U_{10m} > U_o \\ 0 \qquad\qquad\quad , if\ U_{10m} \le U_o \end{cases} \tag{4}$$

- where: $a_{bw} = 0.032$ s/m (constant), U_{10m} is the wind speed at 10 meters above sea level, U_o is the minimum wind speed that starts wave breaking (considered equal to 5 m/s), and T_p is the significant wave period taken from the waves data.

The Weber number (We) helps determine how much inertial forces and oil-water surface tension play a role [33]. It is calculated as:

$$We = \frac{\rho_{sw} g H_s d_o}{\sigma_{ow}} \tag{5}$$

- where: ρ_{sw} is the seawater density (1028 kg/m^3), g is gravity (9.81 m/s^2), H_s is the significant wave height (taken from wave data), σ_{ow} is the oil-water surface tension (0.0313 mN/m and 0.0326 mN/m for two different oil types Arabian Medium, Amoco and Souedie, respectively), d_o is the Rayleigh-Taylor instability maximum diameter [33], given by:

$$d_o = 4\sqrt{\frac{\sigma_{ow}}{g\left(\rho_{sw} - \rho_{oil}\right)}} \tag{6}$$

- where: ρ_{oil} is the oil density (875 kg/m^3 and 903.9 kg/m^3 for Arabian Medium, Amoco and Souedie, respectively).

The Ohnesorge number (Oh) describes the balance between viscous forces and inertial or surface tension forces [33]. It is calculated using the oil's dynamic viscosity ($\mu_{oil} = 20.18$ and 79.5 cPoise for Arabian Medium, Amoco and Souedie, respectively), the oil density, the oil-water surface tension, and the Rayleigh-Taylor instability diameter:

$$Oh = \frac{\mu_{oil}}{\sqrt{\rho_{oil}\sigma_{ow}d_o}} \tag{7}$$

B) Oil resurfacing: Due to buoyancy, oil droplets can rise back to the surface of the water, creating droplets that are either submerged or resurfaced. This process is controlled by the size of the droplets and the difference in density between the oil and the water [33]. Tkalich and Chan [23] noted that resurfacing velocity is calculated differently for small and large droplets. For small droplets, Stokes' law is applied, and for larger droplets, Reynolds' law is used. The vertical terminal velocity $w(r)$ is given by:

$$w(r) = \begin{cases} \sqrt{\frac{16}{3}g(1-\rho)r}, & if\ Re > 50 \\ \frac{2g(1-\rho)}{9v_{sw}}r^2 & ,if\ Re \le 50 \end{cases} \tag{8}$$

- where: r is the droplet radius, $\rho = \rho_{oil}/\rho_{sw}$, v_{sw} is the kinematic water viscosity (= 6.865×10^{-5} m^2/s) and $Re = 2rw(r)/v_{sw}$ is the droplet Reynolds number.

Typical rise speeds for oil droplets vary based on their size and density. For example, a droplet with a diameter of 0.01 mm and a density of 900 kg/m^3 may rise at a rate of about 1 cm per hour, while a droplet with a diameter of 0.5 mm can rise as fast as 30 meters per hour [33]. Additionally, Liu *et al.* [34] present a different terminal velocity, reporting rise speeds up to 0.095 m/s for a 4 mm droplet with a density of 870 kg/m^3.

C) Oil droplet distribution: When an oil droplet is released from a subsea blowout, it starts its slow ascent toward the surface. At this depth, the droplets vary in size—some as small as 0.1 mm (100 μm), others reaching 0.5 mm (500 μm), as described by [35]. Their size determines how quickly they rise; larger droplets buoyantly drift upward, while smaller ones remain suspended, carried by deep-sea currents. The studies of Li *et al.* [31] and Johansen *et al.* [36] have shown that the droplet size distribution is more accurately represented by a lognormal distribution. According to Li *et al.* [31], the volume of the droplet size spectrum is described by the median droplet diameter (D_{50}^V), which can be calculated using the equation:

$$D_{50}^V = d_o r_e (1+10Oh)^p We^q \tag{9}$$

- where: $r_e = 1.791$, $p = 0.46$, and $q = -0.518$ are empirical coefficients [31].

The size distribution follows a lognormal distribution, where the probability density function (*PDF*) is given by:

$$PDF = \frac{1}{ds\sqrt{2\pi}}\exp\left(-\frac{\left(lnd - lnD_{50}^V\right)^2}{2s^2}\right) \tag{10}$$

- where: $s = 0.38 \pm 0.05$ is the standard deviation of the distribution [33].

Finally, the volume size distribution, as described by [37], is:

$$V(d) = d^{-0.7}, d\varepsilon\left[d_{min}, d_{max}\right] \tag{11}$$

- where: d ranges from 1 μm (10^{-6} m) to 1 mm (10^{-3} m).

D) Turbulent mixing: Turbulent mixing redistributes oil droplets vertically, influenced by wind speed, current shear, stratification, and wave energy dissipation. The intensity of turbulent mixing is characterized by a vertical eddy diffusivity coefficient $K(z)$ [38]. In Lagrangian particle tracking the vertical movement of oil droplets can be modeled using a random walk process. This method is based on a stochastic approach, where the movement of particles is influenced by random and deterministic components. The displacement of a particle in the vertical direction (Δz) over a time step (Δt) can be expressed by:

$$\Delta z = K'(z_n)\Delta t + R\sqrt{\frac{2}{r_s}K\left(z_n + \frac{K'(z_n)\Delta t}{2}\right)\Delta t} \tag{12}$$

- where: $K'(z_n)$ is the derivative of the eddy diffusivity coefficient ($K(z)$) with respect to the vertical coordinate (z) at the position of the particle (z_n), R is a random number with a mean of zero ($\mu_{<R^2>} = 0$) and standard deviation of r_s ($\sigma_{<R^2>} = r_s$), the first term represents the non-random advective component, which moves the particle from regions of low diffusivity to regions of high diffusivity and the second term adds the random fluctuation based on the local diffusivity at a position slightly offset from the current particle location [38].

Unlike surface-origin spills, seabed-origin events involve complex vertical transport processes such as buoyant rise, turbulent mixing, and delayed surface detection. The model's ability to simulate oil droplet behavior in the vertical dimension is crucial. Ignoring vertical dynamics—as in many surface-only models—would underrepresent submerged persistence and lead to inaccurate forecasts for seabed spills.

2.3. Oil Weathering Process

OpenOil incorporates advanced parametrizations for oil weathering processes, including (a) dispersion, (b) evaporation, (c) emulsification and (d) biodegradation, leveraging oil properties obtained from the Oil Library (ADIOS) software developed by NOAA. The rate of evaporation varies significantly among different oil types and is influenced by factors such as wind speed [33]. Evaporation and emulsification have notable effects on oil density, viscosity, and oil-water interfacial tension, thereby influencing the droplet size distribution [15].

A) Dispersion: The dispersion process models the entrainment of oil droplets into the water column, driven primarily by turbulence at the ocean surface. This process is a result of wind and wave activity that generates turbulence, causing the oil to mix with the surrounding water [39]. In OpenOil, dispersion is based on the Delvigne and Sweeney algorithms [37], which rely on the calculation of wave energy dissipation. This dissipation represents the energy lost by waves due to breaking and is expressed as:

$$D_e = 0.0034 \times g\rho_{sw}H_s^2 \tag{13}$$

A key factor in this process is the wave energy dissipation coefficient (c_{disp}),

which determines how much of the dissipated wave energy actually contributes to dispersion. It is given by:

$$c_{disp} = \left(D_e\right)^{0.57} f_{bw} \tag{14}$$

- where: f_{bw} (the fraction of breaking waves) is set to 0.02, representing the proportion of waves that break and promote dispersion.

The rate at which oil disperses into the water column (q_{disp}) is calculated using the equation:

$$q_{disp} = \frac{c_{Roy} c_{disp} V_{entrain}}{\rho_{oil}} \tag{15}$$

- where: $c_{Roy} = 2400 \times exp\left(-73.682 \times \sqrt{\frac{\mu_{oil}}{\rho_{oil}}}\right)$ is Roy's constant, which accounts for the interaction between oil and water by adjusting for the oil's viscosity and density, $V_{entrain} = 3.9 \times 10^{-8}$ m^3/s represents the entrainment volume constant, which defines the volume of oil mixed into the water per second.

B) Evaporation: Regarding oil evaporation, OpenOil adapts its treatment based on the conditions of the oil slick [25]. Under calm conditions, where the oil forms a smooth surface, evaporation is modeled using Mackay's analytical method [40]. However, under rough weather conditions, a more complex approach is employed (ADIOS2), which utilizes a pseudo-component evaporation model [41]. In this model, crude oils and refined products are represented as a small number of discrete, non-interacting components, each with its own vapor pressure. The evaporation rate for each component is determined by factors such as wind speed, sea water temperature, slick thickness, and the molar fraction and volume of the component. The relative molar volume of each component is estimated based on empirical correlations with the boiling point of alkanes, allowing for accurate calculation of vapor pressures using Antoine's equation [42].

C) Emulsification: OpenOil computes emulsification through a process as described by [25], which accounts for factors such as the oil's age, evaporation, water fraction, and droplet size distribution. Once emulsification starts, the model calculates the interfacial area (which increases over time) using a rate influenced by wave energy and wind speed. The interfacial area is constrained by the maximum interfacial area (S_{max}) set to 5.4×10^7 m^2, which depends on the oil's properties and droplet sizes. The water fraction (Y) in the emulsion is updated using the relationship between the interfacial area and droplet size, following this equation:

$$Y = \frac{Sd_w}{6 + Sd_w} \tag{16}$$

- where: S is the oil–water interfacial area and d_W is the average water droplet diameter.

D) Biodegradation: Biodegradation is an important natural process that helps reduce the environmental impact of marine oil spills over time. The speed at which oil breaks down depends on factors such as the type of petroleum hydro-

carbons, temperature, the types of microbes present, and the availability of oxygen and nutrients. In OpenOil, the biodegradation model is based on the research of [43]. It suggests that the breakdown of oil is mainly affected by temperature. The total biodegradation time (R^{-1}), in days, is calculated using the following equation:

$$R^{-1} = 12days \times 3^{\left(20^{o}C-T\right)/10^{o}C} \quad (17)$$

- where: R^{-1} is the time, it takes for oil to be colonized by bacteria and microorganisms, and for the most resistant oil compounds to break down and T is the water temperature, considering both dissolved and undissolved oil.

2.4. Numerical Simulation Setup and Study Areas

The numerical simulation for oil spill dispersion was conducted using the OpenOil model, a Lagrangian particle-tracking system integrated with atmospheric and oceanographic forcing data. Two case studies were examined: Baniyas, Syria, for validation purposes, and Zakynthos, Greece, as the primary study area. The model utilized multiple environmental datasets, including wind, hydrodynamics, bathymetry, and wave data, to simulate oil spill trajectories and their interaction with the marine environment, shown in Table 1.

Table 1. Simulation configurations: Parameters and settings used in the oil spill model.

Purpose	Validation	Exploration
Parameter	Baniyas, Syria (2019)	Zakynthos, Ionian Sea (2017)
Date start (UTC)	22 June 23:00	6 August 15:00
Geographical coordinates	35.9060˚E, 35.2224˚N	20.8150˚E, 37.6203˚N
Oil type	Souedie crude oil	Arabian Medium crude oil (Amoco)
Discharge rate	1.588 m^3/h	15.88 m^3/h
Seafloor release	Yes	Yes
Seafloor depth release	40 m	350 m
Total seeding elements	1000	1000
Seeding radius	10 meters	100 meters
Oil spill duration	57 hours	6 hours
Droplet size distribution	0.0001 m - 0.0005 m	0.0001 m - 0.0005 m
Wind drift factors	0% - 6%	0% - 6%
Processes considered	Evaporation, emulsification, dispersion, biodegradation, wind drift, vertical mixing, wave entrainment, coastline stranding	Evaporation, emulsification, dispersion, biodegradation, wind drift, vertical mixing, wave entrainment, coastline stranding
Simulation duration	177 hours (hourly outputs)	258 hours (hourly outputs)

The droplet size range (0.0001 - 0.0005 m) was selected based on values re-

ported in experimental studies of natural and anthropogenic seabed blowouts [21] [35]. The density values correspond to Souedie and Arabian Medium oils, chosen because they represent the most probable oil types involved in the Baniyas and Zakynthos events, respectively, based on local refining and seepage records [18] [19].

To analyze the transport characteristics of simulated oil particles, we implemented a computational approach within the OpenOil python framework. This involved extracting movement data, calculating directional trends, and assessing key transport metrics such as distance and velocity. Longitude and latitude coordinates were retrieved at each time step, and their differences were used to compute displacement, movement angles, and the dominant movement direction. Trajectory characteristics, including total distance traveled, segment-wise distances, and particle velocities, were derived and stored for further analysis. Mean speed and travel distance were also calculated, excluding stationary particles to ensure accuracy. For a detailed implementation, refer to **Appendix A**. The initial release points of the Baniyas and Zakynthos spills were derived from [18] and [19], respectively (**Figure 1**).

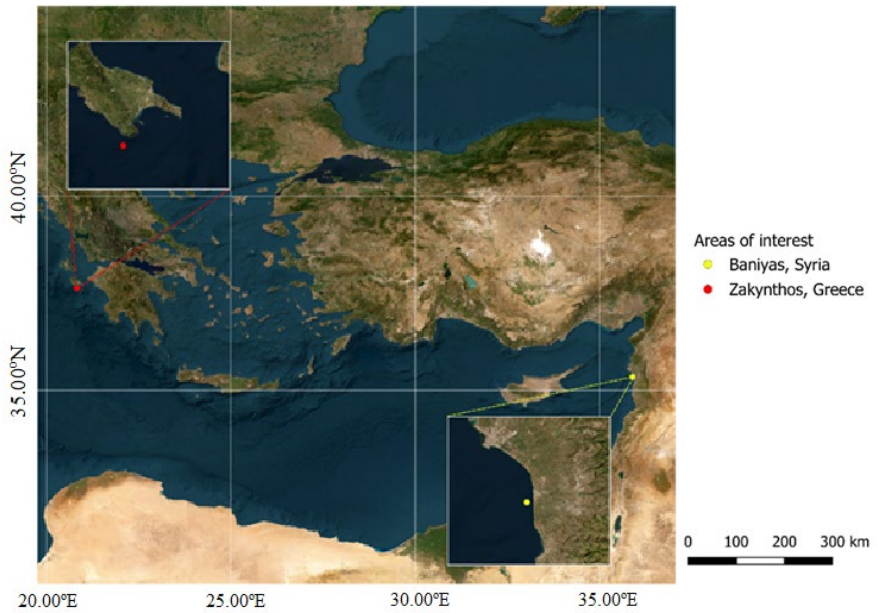

Figure 1. Geographic visualization of the areas of interest. The red marker indicates the initial release point of the Zakynthos oil seep, while the yellow marker denotes the initial release point of the Baniyas oil spill.

3. Results and Discussion

First, we present the validation results concerning the a) Baniyas seabed pipeline sabotage, followed by the exploration of b) Zakynthos physical seafloor oil spill. To support validation and prediction processes, three Sentinel-2 atmospherically corrected images were obtained (two for the Baniyas spill and one for the Zakynthos seepage), ensuring high-quality spectral analysis. All three images are cloud-

free, eliminating distortions and maximizing the accuracy of oil spill detection and extent visualization. The imagery was derived from the Copernicus Data Space Ecosystem browser, providing multispectral data at 10 m, 20 m, and 60 m resolutions, allowing for an optimized analysis of oil slick dispersion and thickness variations [44].

a) Baniyas, Syria: The Sentinel-2 image from June 25, Figure 2(a) shows a large-scale surface oil slick extending offshore from Baniyas, with elongated filamentous structures typical of emulsified oil. By this date, OpenOil simulations indicate that the oil had moved in a mean direction of 16.41˚, at a mean velocity of 3.12 cm/s, covering a mean distance of 4141.5 meters from the point of release (as computed in **Appendix A**).

A direct comparison between the Sentinel-2 image and OpenOil outputs suggests a high degree of accuracy in the simulated oil spill trajectory. The model effectively captures the overall shape, direction, and dispersion of the oil, with the simulated slick extending in the same north-northeastward direction as seen in satellite data. Figure 2(b) illustrates wind conditions on June 25, showing wind speeds between 1.5 - 2.5 m/s. These weak winds contributed to the limited offshore dispersion of the oil, causing it to remain largely confined near the coastline. The agreement between the simulated and observed spill distribution further supports the capability of the model to reproduce oil transport under weak advection conditions.

By June 30, the oil continued to drift north-northeast, with a mean transport direction of 27.68˚. The mean speed increased to 3.97 cm/s, while the mean travel distance increased to 8466.45 meters, reflecting enhanced advection due to changing wind and current patterns.

The Sentinel-2 image from June 30 Figure 3(a) reveals an extended oil slick with increased offshore dispersion, while a portion of the oil has stranded along the coastline. The model accurately simulates this behavior, showing that oil particles continued drifting along the coastline with increasing northward movement, consistent with satellite observations. For the Baniyas case, the deviation between the modeled and observed slick extent was under 600 meters in direction and less than 8% in areal extent, based on pixel-wise overlap between the red overlays in Figure 2(a) and the model outputs. This confirms a close match in both shape and spatial drift pattern.

Figure 3(b) presents wind conditions on June 30, highlighting a rise in wind speeds to 3 - 5 m/s. These stronger winds contributed to greater horizontal advection, leading to the observed increase in oil transport speed and travel distance. At this stage, the simulation showed that 96.1% of the oil particles had stranded along the coastline, with only 3.9% remaining active in the water.

The alignment between OpenOil's predicted oil slick and Sentinel-2 imagery on both dates confirms the reliability of the model in reproducing oil spill dynamics in this region. The observed stranding along the coastline in late June is consistent with model predictions, further validating OpenOil's ability to simulate persistent

oil accumulation in weak current regimes.

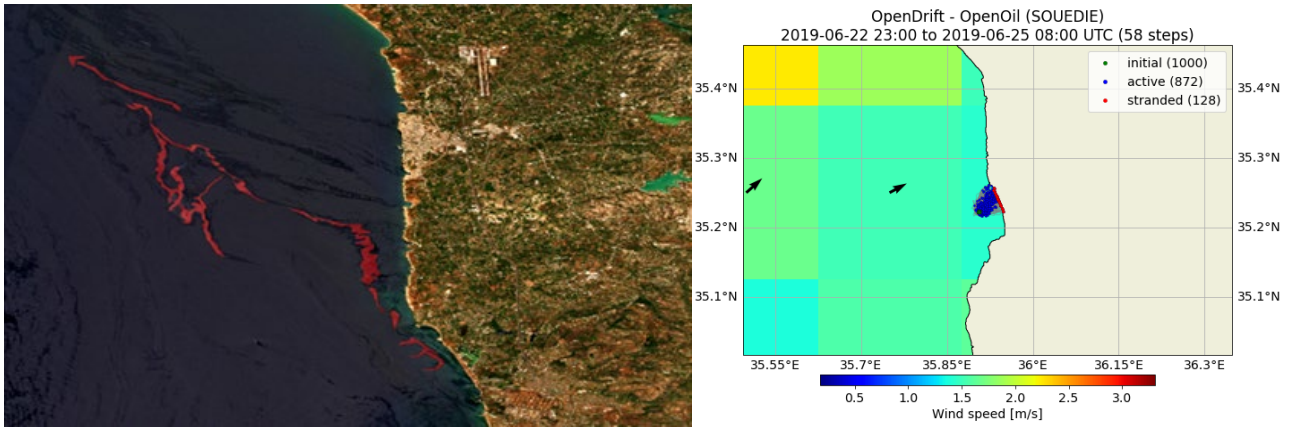

(a) (b)

Figure 2. (a) Sentinel-2 satellite image of the Baniyas oil spill on June 25, 2019. The red overlay indicates the extent of the oil spill, identified using photo-interpretation techniques; (b) Wind speed distribution over the Baniyas open sea region on the same day. Colored points represent oil particles.

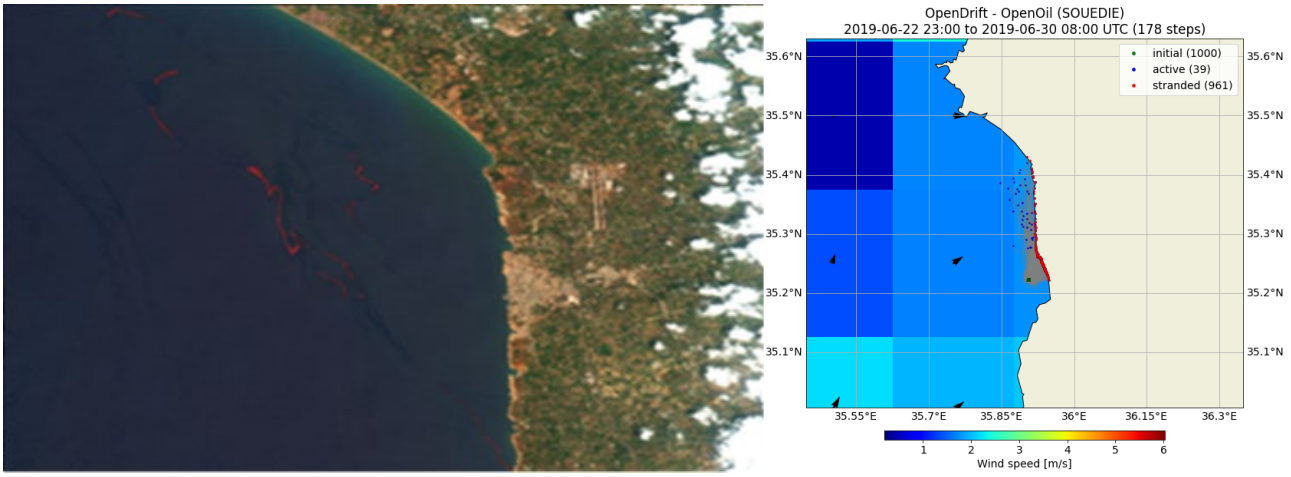

(a) (b)

Figure 3. (a) Sentinel-2 satellite image of the Baniyas oil spill on June 30, 2019. The red overlay indicates the extent of the oil spill, identified using photo-interpretation techniques; (b) Wind speed distribution over the Baniyas open sea region on the same day. Colored points represent oil particles.

b) Zakynthos: A key validation of the OpenOil comes for the Zakynthos spill comes from the Sentinel-2 image captured on August 7, 2017 (**Figure 4**), which is the only available satellite observation where the oil spill is clearly visible. This image provides crucial observational data for assessing the accuracy of the simulated oil spill trajectory. The comparison between the OpenOil simulation and the Sentinel-2 image demonstrates strong agreement, confirming that the modeled oil movement aligns with real-world observations. Both the satellite data and the model output indicate a northeast-to-southwest transport pattern, reflecting the dominant influence of surface currents. Additionally, the elongated shape of oil

slick in the satellite image closely matches the simulated trajectory, suggesting that OpenOil successfully captured the role of constrained flow and eddy formation in oil transport.

Figure 5 illustrates the spreading of oil in relation to ocean currents, with a background color scale ranging from blue (low velocity) to red (high velocity). Black arrows are superimposed on this background, representing the direction and speed of the surface currents. At the onset of the oil spill, the initial movement of the oil particles is primarily influenced by the prevailing ocean currents and wind patterns. The surface currents, moving at speeds ranging from 0.01 to 0.55 m/s, predominantly flow in a northeast-to-southwest direction. This results in a constrained flow, causing the oil particles to accumulate in localized areas near the spill's source. As the oil drifts, it encounters smaller gyres and eddies that trap some of the particles, slowing dispersion in certain regions. These trapped particles linger in circular patterns before eventually being carried away by the southeastward jet of the currents. The presence of these slow-moving eddies adds an element of unpredictability to the spread of the oil, leading to localized clusters before more widespread movement occurs. In addition to the currents, wind plays a crucial role in influencing the oil's dispersion. The winds, which range from 0.5 m/s to 14.4 m/s, with a total average of 3.6 m/s, blow predominantly from the northwest (NW). During periods of stronger winds, the oil is pushed offshore, spreading outward and reducing the concentration near the source. As the spill progresses, nearly all oil particles (~99%) continue to move, further spreading the environmental impact.

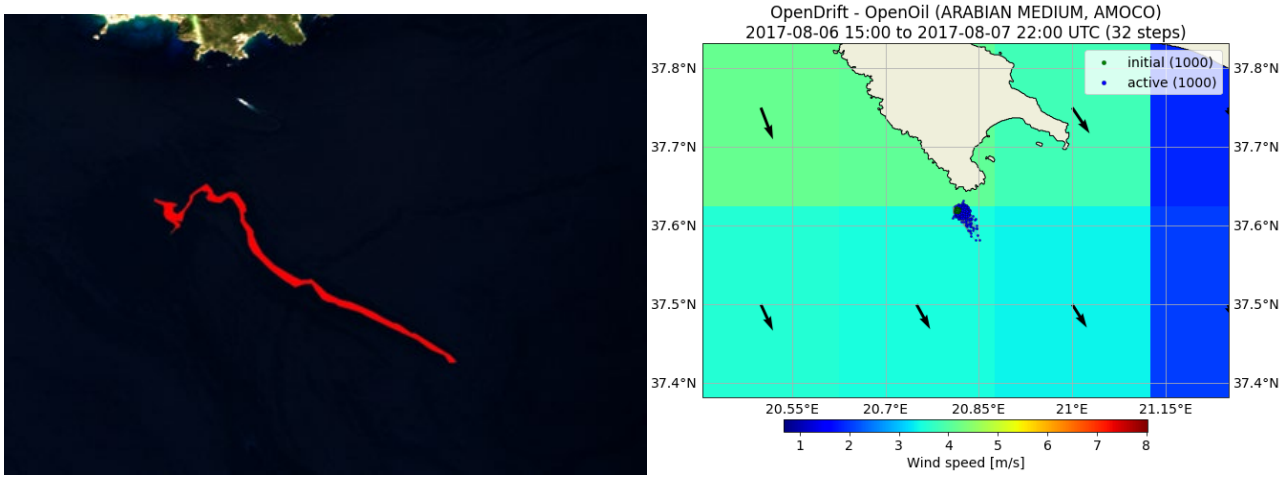

(a) (b)

Figure 4. (a) Sentinel-2 satellite image of the Zakynthos oil spill on August 7, 2017. The red overlay indicates the extent of the oil spill, identified using photo-interpretation techniques; (b) Wind speed distribution over the Zakynthos open sea region on August 7, 2017. Colored points represent oil particles.

Figure 6 illustrates the trajectory of oil particles influenced by wind drift over time. The color gradient represents the wind drift factor, ranging from low (blue) to high (red), demonstrating the varying impact of wind on particle movement.

Initially, oil particles disperse outward, primarily following the prevailing ocean currents, which channel their movement in a northeast-to-southwest direction. As the wind drift factor increases, particles exhibit a more pronounced deviation from the main current flow, extending farther offshore, particularly towards the southeast. This effect is evident in the red-colored trajectories, where higher wind drift factors push oil particles into elongated paths, accelerating their movement away from the spill source. Conversely, lower wind drift factors (blue and green) result in more localized clustering and slower dispersion. The influence of wind is further highlighted by the asymmetry in the spread, where particles subjected to stronger wind drift move more rapidly compared to those primarily driven by ocean currents alone. Over time, these interactions between wind and currents shape the overall dispersion pattern.

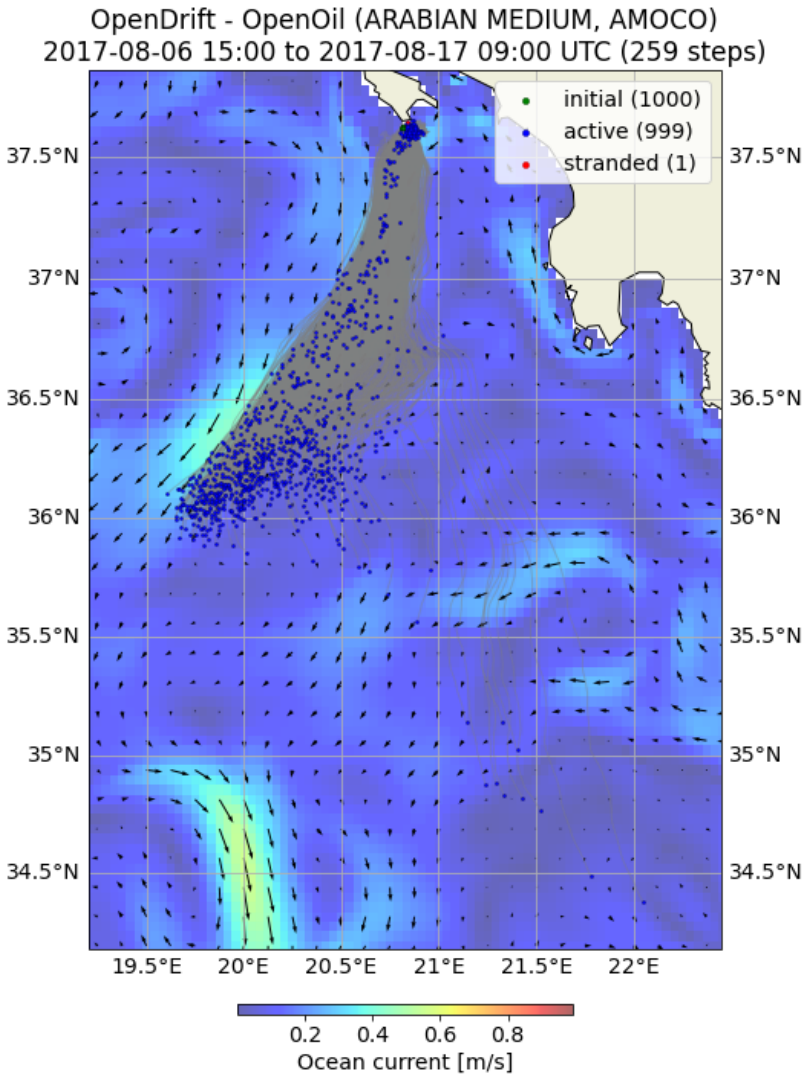

Figure 5. Oil spill transport in Zakynthos after a 258-hour simulation, overlaid with background sea surface current speeds from CMEMS. Green dots indicate the initial positions of the oil elements, blue dots show their positions at the end of the simulation, and gray lines trace their trajectories over time. Red dots represent stranded oil elements.

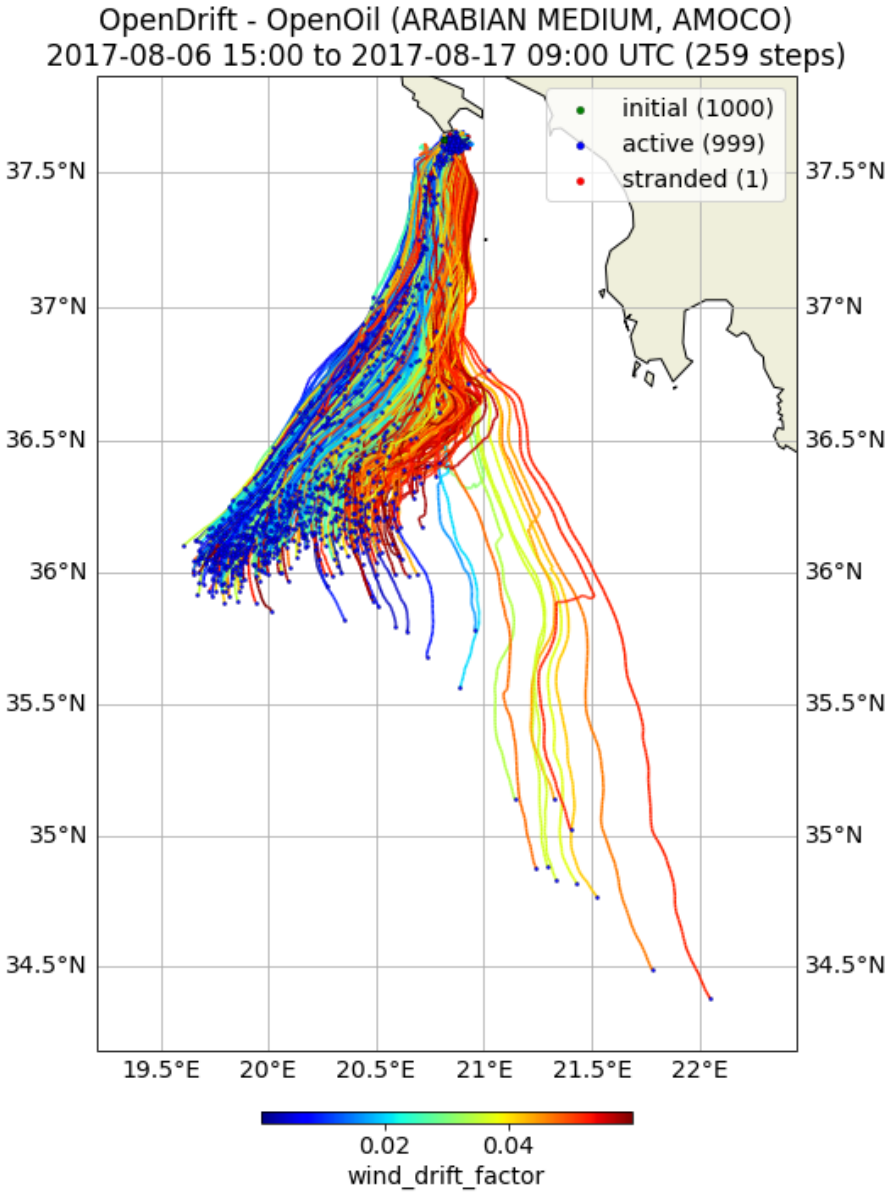

Figure 6. Simulated trajectories of oil particles influenced by wind drift, as computed by the OpenOil model.

Figure 7 presents a detailed analysis of oil droplet size distribution which aligns with the theoretical framework established by [21] [31] [35] and [37]. The histogram in the top-left panel (Figure 7(a)) illustrates the volume spectrum, showing a right-skewed distribution where smaller droplets dominate, while the cumulative volume spectrum (Figure 7(b)) confirms that a majority of the volume is concentrated in these smaller sizes. The middle panels (Figure 7(c)) highlight the number spectrum, demonstrating that the smallest droplets are most numerous, a characteristic consistent with a lognormal distribution. The cumulative number spectrum (Figure 7(d)) further supports this by displaying a rapid rise, indicating that a significant fraction of droplets exists in the smallest size range. The lower

panels, plotted on a logarithmic scale, reveal the power-law behavior of the droplet size distribution (**Figure 7(e)** and **Figure 7(f)**), aligning with the mathematical representation of Equation (11). The comparison with [21] suggests a very close match between the simulated OpenOil results and empirical findings. This analysis underscores the importance of droplet size in determining ascent behavior in subsea blowouts, with smaller droplets being more susceptible to dispersion by deep-sea currents.

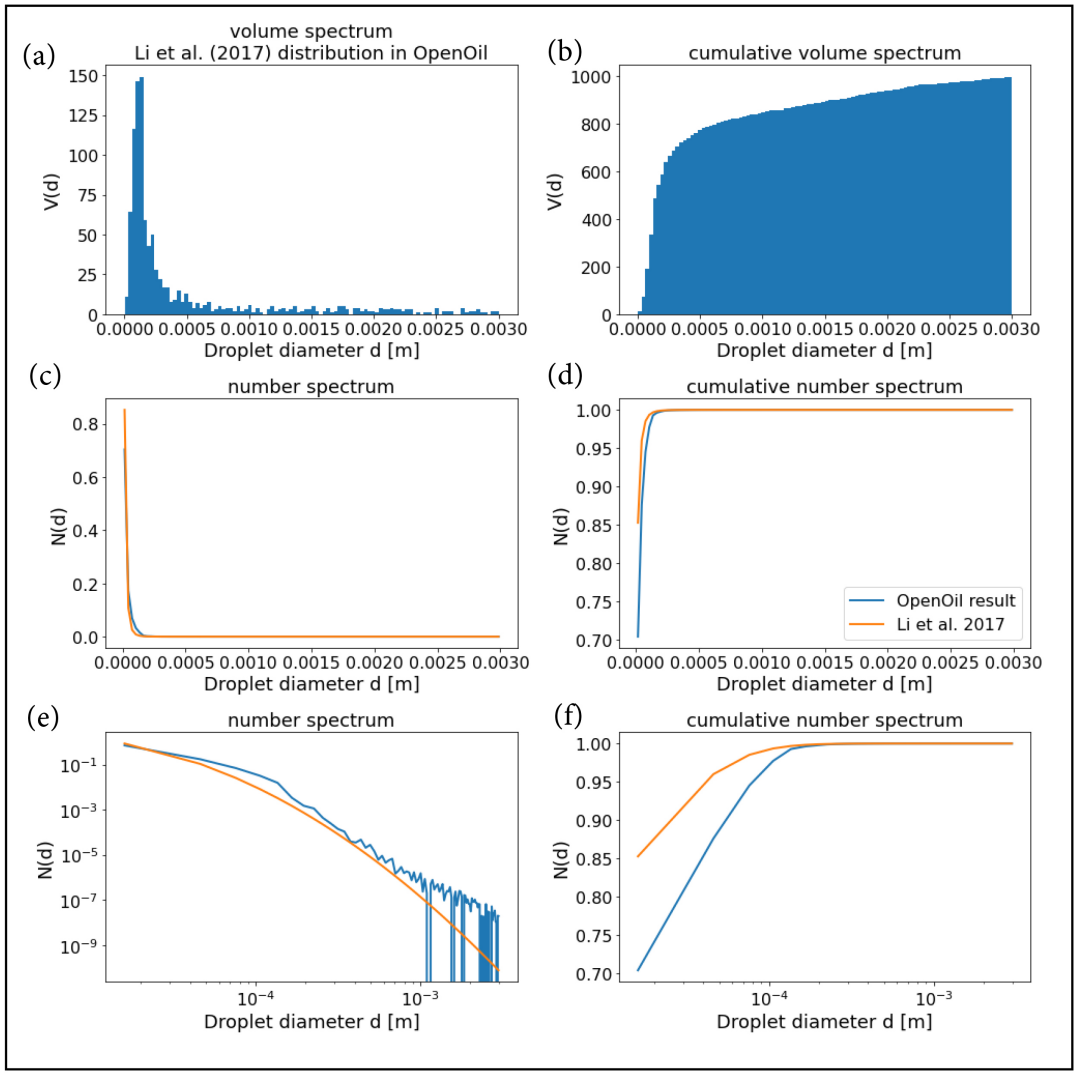

Figure 7. Droplet size distribution analysis: (a) Volume size distribution of oil particles; (b) Distribution of oil droplets by number; (c) Logarithmic distribution of oil droplets by number, simulated by the OpenOil model (blue lines) and by Li *et al.* [21] (orange lines); (d) Cumulative volume size distribution; (e) Cumulative distribution of oil droplets; (f) Logarithmic cumulative distribution of oil droplets.

Figure 8(a) presents the evolution of the oil budget over the course of 258 hours, offering a detailed look at the intricate processes that determine the fate of spilled oil in the ocean. Starting with an initial oil mass exceeding 80,000 kg, the oil undergoes significant transformations driven by physical and chemical forces,

leading to notable changes in its distribution and composition. The oil mass budget per physico-chemical process throughout the simulation time is presented in Table 2. The table illustrates the proportion of oil mass being dispersed, submerged, surface-bound, stranded, and evaporated per 25 hours of simulation, including biodegradation.

Table 2. Oil weathering processes.

Processes/Time (h)	25	50	75	100	125	150	175	200	225	250
Dispersed (%)	3	9	39	48	50	60	68	66	65	65
Submerged (%)	92	63	37	22	13	6	0	0	0	0
Surface (%)	0	15	2	3	6	1	1	1	1	1
Stranded (%)	0	0	0	0	0	0	0	0	0	0
Evaporated (%)	0	1	1	1	1	1	1	1	1	1
Biodegraded (%)	5	12	21	26	30	32	32	32	33	33

Over the course of the 258-hour simulation, the behavior of the oil undergoes significant changes, as reflected in the varying percentages of its different fractions. Initially, the dispersed fraction starts at 3% and gradually increases, peaking at 60% by 150 hours, before stabilizing at 65%. This gradual dispersion of oil is indicative of active mixing by turbulence and wave action, which slows down after the first 50 hours. The submerged oil, which makes up a substantial 92% of the total oil at 25 hours, decreases steadily, eventually reaching 0% by 175 hours. This suggests that the oil gradually moves closer to the surface and is broken down by other processes. Interestingly, biodegradation becomes a dominant factor as the simulation progresses, increasing from 5% at 25 hours to 33% by 250 hours, reflecting the growing activity of microorganisms in breaking down the oil. Evaporation remains minimal throughout, staying consistently low at just 1% after the initial hours. The surface oil fraction fluctuates slightly, peaking at 15% at 50 hours, and then stabilizing at 1% by the end of the simulation. These dynamics are indicative of an oil spill that undergoes significant physical and biological transformations, with the bulk of the oil being gradually biodegraded and dispersed while remaining largely unaffected by evaporation.

In the middle graph (Figure 8(b)), the rising viscosity of the emulsion (green line) is particularly evident after 100 hours, when it reaches over 250,000 cP. This increase in viscosity highlights the growing thickness of the oil as it absorbs more water, transitioning into a more stable emulsion. Interestingly, the water content, represented by the blue shading, begins to rise sharply after 30 hours but levels off at 18% after 80 hours. This suggests that after an initial phase of water absorption, the emulsion stabilizes, and no significant increase in water content occurs beyond this point. This stable water content suggests that the oil has reached a point where it forms a steady emulsified state, becoming increasingly difficult to sepa-

rate from the surrounding water.

The bottom graph (Figure 8(c)) presents wind speed (blue line) and current speed (red line). Wind speeds fluctuate between 0.9 and 12.4 m/s, with an increasing trend that peaks near 150 hours, corresponding with intensified dispersion and emulsification. In contrast, the current speed remains relatively stable, fluctuating between 0.02 and 0.26 m/s, affecting the horizontal transport of the oil.

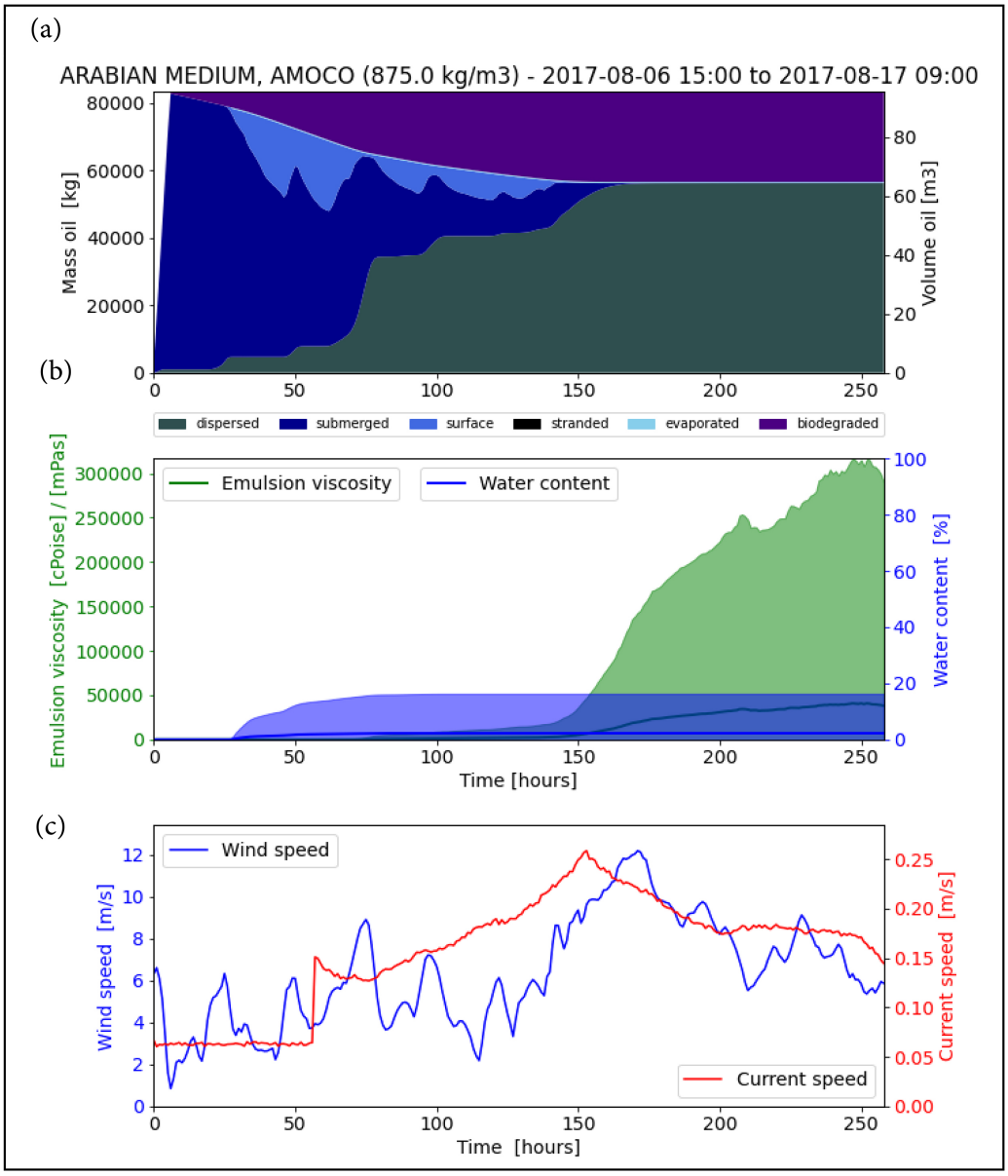

Figure 8. Evolution of the oil budget and environmental processes over time. Time evolution of OpenOil model results for: (a) the oil budget, showing the relative impact of physical and biochemical processes; (b) oil properties, including the mean and standard deviation of oil mass density and viscosity; (c) prevailing wind speed and surface current speed during the 258-hour simulation period.

Figure 9 presents the critical oil density threshold influencing the evaporation

process in a seabed oil spill scenario near Zakynthos. Under the given simulation conditions, oil with a density of 875 kg/m^3 was found to be the critical limit, corresponding to Arabian Medium (AMOCO) with an *API* gravity of 30.07. To determine the *API* gravity, we utilized the ADIOS oil database, applying the specific gravity equation at 15˚C, with $SG = \rho_{oil}/999.1$ and the *API* formula the *API* with $API = (141.5/SG) - 131.5$. The results indicate that for oils with an *API* gravity higher than 30.07 (density lower than 875 kg/m^3), evaporation occurred during the simulation. In contrast, oils with *API* values lower than 30.07 (density greater than 875 kg/m^3) did not exhibit significant evaporation. As shown in Table 3, the oils considered in the simulation ranged from Generic Heavy Crude (density 963 kg/m^3, *API* 15.4) to Generic Light Crude (density 829 kg/m^3, *API* 39.1). The table illustrates the variation in *API* values and densities, highlighting the relationship between oil density and evaporation behavior.

Table 3. Oil types, densities, and corresponding *API* values used to determine the critical evaporation threshold in a seabed oil spill scenario near Zakynthos.

Oil types	Density (kg/m^3)	API
Generic heavy crude	963	15.4
Souedie	904	24.9
Ashtar	881	29
Arabian medium	878	29.5
Arabian medium, exxon	875	30
Arabian medium, amoco	875	30.07
Arabian medium, chevron	875	30.1
Kuwait	871	30.9
Arabian light, shell oil	866	31.8
Generic light crude	829	39.1

Given that oils with *API* gravities higher than 30.07 (density lower than 875 kg/m^3) undergo significant evaporation, and those with lower *API* gravities do not, it is reasonable to assume that the spill's composition includes oils within this mid-range category. This behavior is attributed to the molecular composition and volatility of the oil. Lighter oils (higher *API*) contain more low-molecular-weight hydrocarbons, which are highly volatile and evaporate quickly due to their lower boiling points. In contrast, heavier oils (lower *API*) consist of more high-molecular-weight hydrocarbons, such as resins and asphaltenes, which are less volatile and have higher boiling points, preventing significant evaporation. Additionally, lighter oils spread more easily on the water surface, increasing their exposure to air and enhancing evaporation, whereas heavier oils form thicker layers that limit air-oil interaction, reducing the rate of evaporation [45].

Despite its strengths, OpenOil has some limitations. The model assumes homogeneous mixing conditions and does not currently include sedimentation of oil-

mineral aggregates, which may affect behavior in turbid seabed environments. Its biodegradation rates are simplified and may not represent site-specific microbial communities. Further, droplet breakup at the seafloor is estimated rather than measured, potentially introducing error. These limitations should be considered when applying the model to spills with complex bathymetry, heavy sediment loads, or microbial variability.

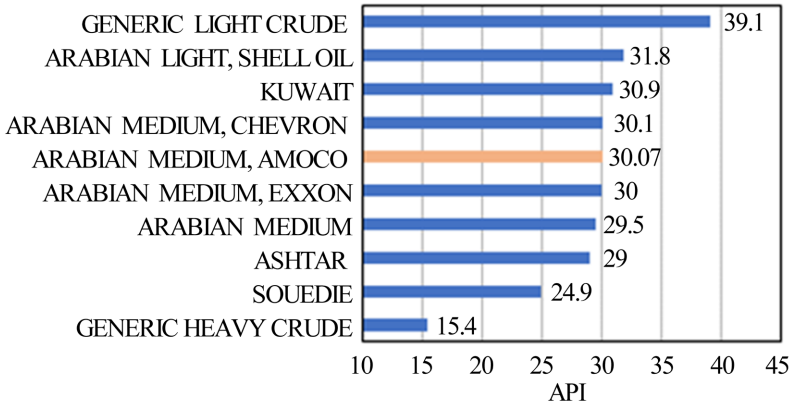

Figure 9. Oil types from the ADIOS database used to test critical density.

4. Conclusions

This study applied OpenDrift's OpenOil module to simulate the transport and fate of oil in seabed-origin spills, with successful validation in both anthropogenic (Baniyas) and natural (Zakynthos) scenarios. The following key findings emerged and are grouped into two categories: (A) insights into the physical behavior of oil released from the seabed under various environmental and compositional conditions, and (B) the performance and capabilities of the OpenOil model in reproducing these complex dynamics with high spatial and temporal fidelity.

A) Physical oil spill behavior

1) Critical Oil Density Threshold for Evaporation: A major insight from the simulations was the identification of 875 kg/m^3 as a critical density threshold governing oil evaporation. Oils with a density below this value—equivalent to an API gravity above 30.07—demonstrated significant evaporation during the simulations. In contrast, denser oils remained largely persistent and non-volatile, even under varying environmental conditions. This threshold provides a valuable indicator for early risk assessment and response prioritization, especially in deep-sea and seabed spill incidents.

2) Evaporation Insignificant in Heavier Oils: Oils such as SOUEDIE and other heavy crude variants exhibited negligible evaporation, regardless of exposure to wind and wave action. This behavior aligns with their high molecular weight composition and confirms that evaporation is not a dominant weathering process for heavy oils released from the seabed. This reinforces the need to rely on other mitigation strategies beyond evaporation-based natural attenuation.

B) Model performance

1) Persistent Nature of Heavy Oil and Modeling Accuracy: The model showed high spatial accuracy in reproducing real-world oil movement patterns. In the case of the Baniyas spill, the simulation results closely matched Sentinel-2 satellite observations, capturing both the limited horizontal spread and the coastal accumulation of oil. These outcomes demonstrate OpenOil's effectiveness in predicting spill behavior in regions with weak currents and low wind energy.

2) Emulsification and Viscosity Changes: OpenOil successfully simulated the emulsification process, revealing that water content in the oil reached up to 18% within 80 hours. This led to a dramatic increase in viscosity, which surpassed 250,000 cP after 100 hours. These changes indicate the formation of a highly viscous, stable emulsion that is more resistant to natural breakdown and mechanical recovery, underlining the importance of modeling time-evolving oil properties for spill response planning.

3) Role of Vertical Mixing and Droplet Size: The simulations revealed that oil droplet size distribution followed a lognormal pattern, as expected from theoretical models. Smaller droplets (≤0.1 mm) remained suspended in the water column for extended periods, while larger ones (>0.3 mm) resurfaced more quickly due to buoyancy. This highlights the critical role of droplet size in determining vertical transport and persistence, emphasizing the need for size-resolved modeling in subsea blowout scenarios. We observed high sensitivity to oil type and droplet size distribution. For instance, simulations with heavier oils (density > 875 kg/m^3) showed negligible evaporation and increased seabed persistence, whereas lighter oils were more prone to dispersion and surface accumulation. Similarly, varying the droplet size range by ±50 μm shifted average resurfacing time by over 30%. These results underscore that seabed spill forecasts are strongly dependent on accurate characterization of oil properties and discharge parameters.

4) Influence of Environmental Forcing: Environmental drivers such as wind and ocean currents significantly influenced oil dispersion patterns. Stronger winds (above 10 m/s) enhanced offshore transport and caused asymmetrical spreading, while eddy structures and local gyres temporarily trapped particles, creating zones of accumulation. These interactions shaped the spatial distribution of oil and contributed to complex transport dynamics beyond simple advection.

5) Model Capabilities and Future Needs: Overall, OpenOil proved to be a robust and reliable tool when integrated with ERA5 reanalysis and CMEMS wave/current data, effectively simulating the multifaceted behavior of oil in seabed-origin spill scenarios. Looking forward, future model improvements should focus on enhancing biodegradation parameterizations to reflect region-specific microbial activity, and on refining droplet size distribution algorithms based on *in-situ* observations, to further increase modeling fidelity.

Acknowledgements

Portions of this work were previously included in project deliverables submitted

under the framework of the WATERVERSE initiative.

Author Contributions

V.P. conceived the study and wrote the abstract; **V.P.** and **C.A.** wrote introduction, methodology and results; **A.M.** and **K.V.** reviewed the first draft; **A.M.**, **I.G.**, **S.V.** and **I.K.** supervised the methodology and conclusions sections. All authors have read and agreed to the published version of the manuscript.

Conflicts of Interest

The authors declare no conflict of interest.

References

[1] ITOPF (2024) Oil Tanker Spill Statistics 2024. https://www.itopf.org/knowledge-resources/data-statistics/statistics/

[2] Carpenter, A. and Kostianoy, A.G. (2018) Oil Pollution in the Mediterranean Sea: Part I: The International Context. The Handbook of Environmental Chemistry, Vol. 83, Springer. https://doi.org/10.1007/978-3-030-12236-2

[3] Chen, H., An, W., You, Y., Lei, F., Zhao, Y. and Li, J. (2015) Numerical Study of Underwater Fate of Oil Spilled from Deepwater Blowout. *Ocean Engineering*, **110**, 227-243. https://doi.org/10.1016/j.oceaneng.2015.10.025

[4] French-McCay, D.P., Robinson, H.J., Spaulding, M.L., Li, Z., Horn, M., Gloekler, M.D., *et al.* (2021) Validation of Oil Fate and Mass Balance for the Deepwater Horizon Oil Spill: Evaluation of Water Column Partitioning. *Marine Pollution Bulletin*, **173**, Article ID: 113064. https://doi.org/10.1016/j.marpolbul.2021.113064

[5] Wang, Y., Lee, K., Liu, D., Guo, J., Han, Q., Liu, X., *et al.* (2020) Environmental Impact and Recovery of the Bohai Sea Following the 2011 Oil Spill. *Environmental Pollution*, **263**, Article ID: 114343. https://doi.org/10.1016/j.envpol.2020.114343

[6] Keramea, P., Spanoudaki, K., Zodiatis, G., Gikas, G. and Sylaios, G. (2021) Oil Spill Modeling: A Critical Review on Current Trends, Perspectives, and Challenges. *Journal of Marine Science and Engineering*, **9**, Article No. 181. https://doi.org/10.3390/jmse9020181

[7] Papaioannou, V., *et al.* (2025) Assessment of Oil Spill Dispersion and Weathering Processes in Saronic Gulf. *Advances in Hydrology & Meteorology*, **2**, Article ID: 000550. https://doi.org/10.33552/ahm.2025.02.000550

[8] Fingas, M. (2017) *In Situ* Burning: An Update. In: Fingas, M., Ed., *Oil Spill Science and Technology*, Elsevier, 483-676. https://doi.org/10.1016/b978-0-12-809413-6.00010-2

[9] Simecek-Beatty, D. and Lehr, W.J. (2017) Extended Oil Spill Spreading with Langmuir Circulation. *Marine Pollution Bulletin*, **122**, 226-235. https://doi.org/10.1016/j.marpolbul.2017.06.047

[10] Zafirakou, A. (2019) Oil Spill Dispersion Forecasting Models. In: Fouzia, H.B., Ed., *Monitoring of Marine Pollution*, IntechOpen, 3-5. https://doi.org/10.5772/intechopen.81764

[11] Daling, P.S., Moldestad, M.Ø., Johansen, Ø., Lewis, A. and Rødal, J. (2003) Norwegian Testing of Emulsion Properties at Sea—The Importance of Oil Type and Release Conditions. *Spill Science & Technology Bulletin*, **8**, 123-136. https://doi.org/10.1016/s1353-2561(03)00016-1

[12] McGenity, T.J., Folwell, B.D., McKew, B.A. and Sanni, G.O. (2012) Marine Crude-Oil Biodegradation: A Central Role for Interspecies Interactions. *Aquatic Biosystems*, **8**, Article No. 10. https://doi.org/10.1186/2046-9063-8-10

[13] Ward, C.P., Sharpless, C.M., Valentine, D.L., French-McCay, D.P., Aeppli, C., White, H.K., *et al.* (2018) Partial Photochemical Oxidation Was a Dominant Fate of *Deepwater Horizon* Surface Oil. *Environmental Science & Technology*, **52**, 1797-1805. https://doi.org/10.1021/acs.est.7b05948

[14] Dagestad, K., Röhrs, J., Breivik, Ø. and Ådlandsvik, B. (2018) OpenDrift v1.0: A Generic Framework for Trajectory Modelling. *Geoscientific Model Development*, **11**, 1405-1420. https://doi.org/10.5194/gmd-11-1405-2018

[15] Hole, L.R., Dagestad, K., Röhrs, J., Wettre, C., Kourafalou, V.H., Androulidakis, Y., *et al.* (2019) The Deepwater Horizon Oil Slick: Simulations of River Front Effects and Oil Droplet Size Distribution. *Journal of Marine Science and Engineering*, **7**, Article No. 329. https://doi.org/10.3390/jmse7100329

[16] Androulidakis, Y., Kourafalou, V., Robert Hole, L., Le Hénaff, M. and Kang, H. (2020) Pathways of Oil Spills from Potential Cuban Offshore Exploration: Influence of Ocean Circulation. *Journal of Marine Science and Engineering*, **8**, Article No. 535. https://doi.org/10.3390/jmse8070535

[17] Keramea, P., Kokkos, N., Zodiatis, G., Sylaios, G., Coppini, G., Peña, J., Benjumeda Herreros, P., Sepp-Neves, A.A., Lardner, R., Liubartseva, S., Soloviev, D., Scuro, M., Nicolaidis, A. and Viola, F. (2023) Oil Spill Modeling Assessment of the 2021 Syrian Oil Spill Using SAR Imagery and Multi-Forcing Forecasts. *EGU General Assembly* 2023, Vienna, 23-28 April 2023, EGU23-1573. https://doi.org/10.5194/egusphere-egu23-1573

[18] Zwijnenburg, W. (2019) Iranian Oil Spills on Syria's Shores: A Brief OSINT Overview of an Environmental Incident. https://www.bellingcat.com/news/mena/2019/07/31/iranian-oil-spills-on-syrias-shores-a-brief-osint-overview-of-an-environmental-incident/

[19] Kolokoussis, P. and Karathanassi, V. (2018) Oil Spill Detection and Mapping Using Sentinel 2 Imagery. *Journal of Marine Science and Engineering*, **6**, Article No. 4. https://doi.org/10.3390/jmse6010004

[20] Rigakis, N., Nikolaou, K., Marnelis, F. and Pakos, T. (2007) The Utility of Oil Shows in the Hydrocarbon Exploration of Western Greece. *Bulletin of the Geological Society of Greece*, **40**, 959-971. https://doi.org/10.12681/bgsg.16779

[21] Li, C., Miller, J., Wang, J., Koley, S.S. and Katz, J. (2017) Size Distribution and Dispersion of Droplets Generated by Impingement of Breaking Waves on Oil Slicks. *Journal of Geophysical Research*: *Oceans*, **122**, 7938-7957. https://doi.org/10.1002/2017jc013193

[22] Serra, T., Granata, T., Colomer, J., Stips, A., Møhlenberg, F. and Casamitjana, X. (2003) The Role of Advection and Turbulent Mixing in the Vertical Distribution of Phytoplankton. *Estuarine*, *Coastal and Shelf Science*, **56**, 53-62. https://doi.org/10.1016/s0272-7714(02)00120-8

[23] Tkalich, P. and Chan, E.S. (2002) Vertical Mixing of Oil Droplets by Breaking Waves. *Marine Pollution Bulletin*, **44**, 1219-1229. https://doi.org/10.1016/s0025-326x(02)00178-9

[24] Azevedo, A., Oliveira, A., Fortunato, A.B., Zhang, J. and Baptista, A.M. (2014) A Cross-Scale Numerical Modeling System for Management Support of Oil Spill Accidents. *Marine Pollution Bulletin*, **80**, 132-147. https://doi.org/10.1016/j.marpolbul.2014.01.028

[25] Lehr, W., Jones, R., Evans, M., Simecek-Beatty, D. and Overstreet, R. (2002) Revisions of the ADIOS Oil Spill Model. *Environmental Modelling & Software*, **17**, 189-197. https://doi.org/10.1016/s1364-8152(01)00064-0

[26] Hersbach, H., Bell, B., Berrisford, P., Biavati, G., Horányi, A., Muñoz Sabater, J., Nicolas, J., Peubey, C., Radu, R., Rozum, I., Schepers, D., Simmons, A., Soci, C., Dee, D. and Thépaut, J.-N. (2023) ERA5 Hourly Data on Single Levels from 1940 to Present. Copernicus Climate Change Service (C3S) Climate Data Store (CDS).

[27] Escudier, R., Clementi, E., Omar, M., Cipollone, A., Pistoia, J., Aydogdu, A., Drudi, M., Grandi, A., Lyubartsev, V., Lecci, R., Cretí, S., Masina, S., Coppini, G. and Pinardi, N. (2020) Mediterranean Sea Physical Reanalysis (CMEMS MED-Currents) (Version 1) [Data Set]. Copernicus Monitoring Environment Marine Service (CMEMS). https://doi.org/10.25423/CMCC/MEDSEA_MULTIYEAR_PHY_006_004_E3R1

[28] Korres, G., Oikonomou, C., Denaxa, D. and Sotiropoulou, M. (2023) Mediterranean Sea Waves Analysis and Forecast (Copernicus Marine Service MED-Waves, MED-WAM4 System) (Version 1) [Data Set]. Copernicus Marine Service (CMS). https://doi.org/10.25423/cmcc/medsea_analysisforecast_wav_006_017_medwam4

[29] Breivik, Ø., Bidlot, J. and Janssen, P.A.E.M. (2016) A Stokes Drift Approximation Based on the Phillips Spectrum. *Ocean Modelling*, **100**, 49-56. https://doi.org/10.1016/j.ocemod.2016.01.005

[30] Lamarre, E. and Melville, W.K. (1991) Air Entrainment and Dissipation in Breaking Waves. *Nature*, **351**, 469-472. https://doi.org/10.1038/351469a0

[31] Li, Z., Spaulding, M.L. and French-McCay, D. (2017) An Algorithm for Modeling Entrainment and Naturally and Chemically Dispersed Oil Droplet Size Distribution under Surface Breaking Wave Conditions. *Marine Pollution Bulletin*, **119**, 145-152. https://doi.org/10.1016/j.marpolbul.2017.03.048

[32] Keramea, P., Kokkos, N., Gikas, G. and Sylaios, G. (2022) Operational Modeling of North Aegean Oil Spills Forced by Real-Time Met-Ocean Forecasts. *Journal of Marine Science and Engineering*, **10**, Article No. 411. https://doi.org/10.3390/jmse10030411

[33] Röhrs, J., Dagestad, K., Asbjørnsen, H., Nordam, T., Skancke, J., Jones, C.E., *et al.* (2018) The Effect of Vertical Mixing on the Horizontal Drift of Oil Spills. *Ocean Science*, **14**, 1581-1601. https://doi.org/10.5194/os-14-1581-2018

[34] Liu, R., Boufadel, M.C., Zhao, L., Nedwed, T., Lee, K., Marcotte, G., *et al.* (2022) Oil Droplet Formation and Vertical Transport in the Upper Ocean. *Marine Pollution Bulletin*, **176**, Article ID: 113451. https://doi.org/10.1016/j.marpolbul.2022.113451

[35] Johansen, Ø. (2003) Development and Verification of Deep-Water Blowout Models. *Marine Pollution Bulletin*, **47**, 360-368. https://doi.org/10.1016/s0025-326x(03)00202-9

[36] Johansen, Ø., Reed, M. and Bodsberg, N.R. (2015) Natural Dispersion Revisited. *Marine Pollution Bulletin*, **93**, 20-26. https://doi.org/10.1016/j.marpolbul.2015.02.026

[37] Delvigne, G.A.L. and Sweeney, C.E. (1988) Natural Dispersion of Oil. *Oil and Chemical Pollution*, **4**, 281-310. https://doi.org/10.1016/s0269-8579(88)80003-0

[38] Visser, A. (1997) Using Random Walk Models to Simulate the Vertical Distribution of Particles in a Turbulent Water Column. *Marine Ecology Progress Series*, **158**, 275-281. https://doi.org/10.3354/meps158275

[39] Wang, C., Han, L., Zhang, Y., Jiang, A., Wang, J. and Niu, X. (2023) Effects of Physical Properties and Environmental Conditions on the Natural Dispersion of Oil. *Journal*

of Marine Science and Engineering, **12**, Article No. 47. https://doi.org/10.3390/jmse12010047

[40] Stiver, W. and Mackay, D. (1984) Evaporation Rate of Spills of Hydrocarbons and Petroleum Mixtures. *Environmental Science & Technology*, **18**, 834-840. https://doi.org/10.1021/es00129a006

[41] Jones, R. K. (1997) A Simplified Pseudo-Component Oil Evaporation Model. *Proceedings of the* 20*th Arctic and Marine Oil Spill Program Technical Seminar*, Vancouver, 11-13 June 1997, 43-61. https://inis.iaea.org/search/search.aspx?orig_q=RN:29000027

[42] Devis Morales, A., Rodríguez Rubio, E. and Rincón Martínez, D. (2022) Numerical Modeling of Oil Spills in the Gulf of Morrosquillo, Colombian Caribbean. *CT&F—Ciencia, Tecnología y Futuro*, **12**, 69-83. https://doi.org/10.29047/01225383.396

[43] Adcroft, A., Hallberg, R., Dunne, J.P., Samuels, B.L., Galt, J.A., Barker, C.H., *et al.* (2010) Simulations of Underwater Plumes of Dissolved Oil in the Gulf of Mexico. *Geophysical Research Letters*, **37**, L18605. https://doi.org/10.1029/2010gl044689

[44] European Space Agency (ESA) (2024) Copernicus Sentinel Data. https://dataspace.copernicus.eu/

[45] Fingas, M.F. (1997) Studies on the Evaporation of Crude Oil and Petroleum Products: I. The Relationship between Evaporation Rate and Time. *Journal of Hazardous Materials*, **56**, 227-236. https://doi.org/10.1016/s0304-3894(97)00050-2

Appendix A: Numerical Simulation Code

The following Python script was implemented within the OpenOil framework to calculate movement direction, trajectory lengths, and speed metrics for the simulated oil particles.

```
#%%
# Assuming o.get_lonlats() returns lon and lat
lon, lat = o.get_lonlats()
# Calculate longitude and latitude differences between consecutive time steps
lon_diff = np.diff(lon)
lat_diff = np.diff(lat)
# Calculate the angle (direction) of each movement in radians
movement_angles = np.arctan2(lat_diff, lon_diff)
# Convert angles from radians to degrees
movement_directions_deg = np.degrees(movement_angles)
# Calculate the mean direction (dominant direction)
mean_direction_deg = np.mean(movement_directions_deg)
# Convert the mean direction to the range [0, 360) degrees
mean_direction_deg = (mean_direction_deg + 360) % 360
# Assuming o.get_trajectory_lengths() returns a tuple with total distance, distances during each time step, and speed
total_distance, distances, speeds = o.get_trajectory_lengths()
# Save total distance to a file
np.savetxt('/home/vaspapa/opendrift/Syria_SOUEDIE/total_distance.txt', total_distance, header = 'total_distance', delimiter=' ')
# Save distances to a file
np.savetxt('/home/vaspapa/opendrift/Syria_SOUEDIE/distances.txt', distances, header='distances', delimiter=' ')
# Save speeds to a file
np.savetxt('/home/vaspapa/opendrift/Syria_SOUEDIE/speeds.txt', speeds, header='speeds', delimiter=' ')
# Calculate mean speed excluding zero values
non_zero_speeds = speeds[speeds != 0]
mean_speed = np.mean(non_zero_speeds)
# Calculate mean distance
mean_distance = np.mean(total_distance)
# Combine lat, lon, and total distance into a single array
data = np.column_stack((lat, lon, total_distance))
# Save the data to an ASCII file
np.savetxt('/home/vaspapa/opendrift/Syria_SOUEDIE/particle_data.txt', data, header='lat lon length', delimiter=' ')
# Print mean speed, distance and the mean direction
print(f"Mean Direction: {mean_direction_deg} degrees")
```

```
print(f"Mean Speed (excluding zeros): {mean_speed}")
print(f"Mean Distance: {mean_distance}")
#%%
```